EUROPEAN TRANSACTIONS ON ELECTRICAL POWER
Euro. Trans. Electr. Power 2010; **20**:611–629
Published online 20 April 2009 in Wiley InterScience
(www.interscience.wiley.com) DOI: 10.1002/etep.342

Modelling and simulation of stator and rotor fault conditions in induction machines for testing fault diagnostic techniques

Shuo Chen*,† and Rastko Živanović

School of Electrical & Electronic Engineering, University of Adelaide, Australia

SUMMARY

On-line diagnostics of induction machine faults such as broken rotor bars and shorted stator windings can be accomplished by analysing the anomalies of machine stator current. Defective rotor bars result in twice slip frequency sidebands around the fundamental frequency in the stator current, while stator winding short circuits cause changes in stator current amplitude and the occurrence of negative sequence current. This paper presents an induction machine model based on the Coupled Circuit Approach to simulate both the rotor and stator faults in an induction machine and to test fault diagnostic techniques. This model is realized in Matlab/Simulink and its construction in Simulink is explained with sufficient details. Simulation results of both the rotor and stator fault conditions are presented. A novel high-resolution spectral analysis approach and a technique based on Discrete Fourier Transform (DFT) for the detection of broken rotor bars are tested using the simulated data. The results confirm that the high-resolution method overcomes drawbacks of DFT such as the requirement for long data windows. Copyright © 2009 John Wiley & Sons, Ltd.

KEY WORDS: induction machine; fault diagnostics; model; broken rotor bar; short circuited windings; high-resolution

1. INTRODUCTION

Induction machines are the prime movers of industry. Generally, they are robust and reliable. However, due to the combination of working environment and installation and manufacturing factors, internal faults frequently occur on rotor bars and stator windings. Broken rotor bars and shorted stator windings are some of the most common rotor and stator faults. They not only reduce the machine working efficiency, but also are potential hazards for production continuity and safety. In the last few decades, considerable research has been undertaken in the area of induction machine condition monitoring and fault diagnostics. Many of them are within the topic of the detection of broken rotor bars and shorted stator turns [1–4].

In this paper, we introduce a model-based tool for research and testing of induction machine fault diagnostic methods. Model based research has the advantage of less financial and manpower costs, and the flexibility of modifying all parameters. Thus, it allows and simplifies comprehensive and systematic studies. A number of models have been proposed for investigations of fault conditions on induction motors [5–9]. However, most of them are either too complex or can only simulate one specific fault. The aim of this paper is to present a useful and simple model to simulate both induction machine stator and rotor asymmetry faults for the purpose of testing fault diagnostic methods. The model is based on the Coupled Circuit Approach incorporating the orthogonal or $qd0$ reference frame theory. It has the advantages of relatively lower complexity and is able to model both rotor and stator faults. The implementation of the model is accomplished in Matlab/Simulink, which is a widely-adopted scientific simulation platform.

Broken rotor bars in an induction machine can be detected by the presence of sideband frequencies in the stator current spectrum using Machine Current Signature Analysis (MCSA) [10]. The classical detection approach in MCSA is based on Discrete Fourier Transform (DFT). However, inherent drawbacks of DFT, such as the impact of side lobe leakage [11] and the requirement of long data windows have made the detection of broken rotor bars troublesome in some cases [12,13]. This paper proposes a novel

*Correspondence to: Shuo Chen, School of Electrical & Electronic Engineering, The University of Adelaide, SA 5005, Australia.
†E-mail: chen.shuo@yahoo.com

high-resolution spectral analysis technique which outperforms DFT in the diagnostics of broken rotor bars. This method is able to maintain a high resolution in the frequency domain while using a considerably small data window.

In Section 2, the theory of Coupled Circuit Approach for modelling an induction machine is firstly reviewed. The systems of differential equations governing the induction machine behaviours under healthy, rotor fault and stator fault conditions are then detailed mathematically. After this, the implementation of the model in Matlab/Simulink is explained and illustrated in Section 3. To verify the model, laboratory experiments are conducted and the results are presented and compared in Section 4. In Section 5, common rotor and stator fault indictors in simulation result are presented. Diagnosis of broken rotor bars using high-resolution spectral analysis is tested and its advantage compared to DFT is demonstrated.

2. COUPLED CIRCUIT APPROACH BASED MODELLING OF INDUCTION MACHINES WITH ROTOR AND STATOR FAULTS

The aim of this section is to present the system of differential equations of the induction machine in the healthy, the broken rotor bars and the shorted stator windings conditions. The Coupled Circuit Approach combined with the Arbitrary Reference Frames theory is the theoretical groundwork for modelling induction machines [14,15]. The balanced electromagnetic relationships of an induction machine are first described mathematically in the *abc* reference frame, and then transformed to an arbitrary rotating reference frame. An induction machine is a highly symmetrical electromagnetic system. Any fault will induce a certain degree of asymmetry. Therefore, broken rotor bars and shorted stator windings are modelled by unbalancing the rotor and stator parameters in certain manners, accordingly [16–18].

2.1. Model of healthy induction machine

In this paper, the model of an induction machine in balanced condition is developed based on a model proposed in Reference [19]. The system of winding equations may be presented in terms of the first-order differential equations of the voltages in the *abc* reference frame as [15]

$$\mathbf{u}_s^{abc} = \mathbf{r}_s\, \mathbf{i}_s^{abc} + \frac{\mathrm{d}\,\lambda_s^{abc}}{\mathrm{d}t} \tag{1}$$

$$\mathbf{u}_r^{abc} = \mathbf{r}_r\, \mathbf{i}_r^{abc} + \frac{\mathrm{d}\,\lambda_r^{abc}}{\mathrm{d}t} \tag{2}$$

and

$$\lambda_s^{abc} = \mathbf{L}_{ss}^{abc}\, \mathbf{i}_s^{abc} + \mathbf{L}_{sr}^{abc}\, \mathbf{i}_r^{abc} \tag{3}$$

$$\lambda_r^{abc} = \mathbf{L}_{rr}^{abc}\, i_r^{abc} + \mathbf{L}_{rs}^{abc}\, \mathbf{i}_s^{abc} \tag{4}$$

Notations $\mathbf{u}_s^{abc}$, $\mathbf{i}_s^{abc}$, λ_s^{abc}, $\mathbf{u}_r^{abc}$, $\mathbf{i}_r^{abc}$ and λ_r^{abc} are column vectors representing the voltages, currents and flux linkages of each phase in either stator or rotor, where the subscripts *s* and *r* indicate stator and rotor, respectively, and the superscript *abc* denotes the three phases.

In an ideal induction machine, the resistances in each stator or rotor phase are assumed to be equal. Thus, notations $\mathbf{r}_s$ and $\mathbf{r}_r$ are diagonal matrices with one phase equivalent resistance of the stator or rotor, whichever the subscript indicates, as the non-zero elements. $\mathbf{L}_{ss}^{abc}$ and $\mathbf{L}_{rr}^{abc}$ are symmetrical matrices of the self inductance of the stator and the rotor windings, and $\mathbf{L}_{sr}^{abc}$ and $\mathbf{L}_{rs}^{abc}$ are symmetrical matrices of the stator-to-rotor and rotor-to-stator mutual inductances, respectively.

The stator and rotor voltage equations are coupled to one another through the mutual inductance terms, which are a function of the rotor angle θ_r. Thus, the coupled terms interact and vary with the rotor position and time. By transforming the equations from *abc* reference frame to an arbitrary rotating *qd*0 reference frame, all the motor variables are in the same coordinate system [19]. If θ is the angle between the *q*-axis and the *a*-axis of the two reference frames, respectively, the matrix which transforms the variables from *abc*

DOI: 10.1002/etep

to $qd0$ reference frame is defined as [19]

$$\mathbf{T}_{qd0}(\theta) = \frac{2}{3}\begin{bmatrix} \cos\theta & \cos(\theta - \frac{2\pi}{3}) & \cos(\theta + \frac{2\pi}{3}) \\ \sin\theta & \sin(\theta - \frac{2\pi}{3}) & \sin(\theta + \frac{2\pi}{3}) \\ \frac{1}{2} & \frac{1}{2} & \frac{1}{2} \end{bmatrix} \tag{5}$$

Equations (1)–(4) then can be transformed to the $qd0$ reference frame, yielding

$$\mathbf{u}_s^{qd0} = \mathbf{r}_s^{qd0}\mathbf{i}_s^{qd0} + \mathbf{E}_s^{qd0} + \frac{\mathrm{d}\lambda_s^{qd0}}{\mathrm{d}t} \tag{6}$$

$$\mathbf{u}_r^{qd0} = \mathbf{r}_r^{qd0}\mathbf{i}_r^{qd0} + \mathbf{E}_r^{qd0} + \frac{\mathrm{d}\lambda_r^{qd0}}{\mathrm{d}t} \tag{7}$$

where $\mathbf{E}_s^{qd0} = \omega\begin{bmatrix} 0 & 1 & 0 \\ -1 & 0 & 0 \\ 0 & 0 & 0 \end{bmatrix}\lambda_s^{qd0}$, $\mathbf{E}_r^{qd0} = (\omega - \omega_r)\begin{bmatrix} 0 & 1 & 0 \\ -1 & 0 & 0 \\ 0 & 0 & 0 \end{bmatrix}\lambda_r^{qd0}$, $\omega = \frac{\mathrm{d}\theta}{\mathrm{d}t}$ and $\omega_r = \frac{\mathrm{d}(\theta_r)}{\mathrm{d}t}$

Resistance and flux linkage matrices in the $qd0$ reference frame are

$$\mathbf{r}_{s,r}^{qd0} = r_{s,r}\begin{bmatrix} 1 & 0 & 0 \\ 0 & 1 & 0 \\ 0 & 0 & 1 \end{bmatrix} \tag{8}$$

and

$$\begin{bmatrix} \lambda_s^{qd0} \\ \lambda_r'^{qd0} \end{bmatrix} = \begin{bmatrix} L_{ls}+L_m & 0 & 0 & L_m & 0 & 0 \\ 0 & L_{ls}+L_m & 0 & 0 & L_m & 0 \\ 0 & 0 & L_{ls} & 0 & 0 & 0 \\ L_m & 0 & 0 & L'_{lr}+L_m & 0 & 0 \\ 0 & L_m & 0 & 0 & L'_{lr}+L_m & 0 \\ 0 & 0 & 0 & 0 & 0 & L'_{lr} \end{bmatrix}\begin{bmatrix} \mathbf{i}_s^{qd0} \\ \mathbf{i}_r'^{qd0} \end{bmatrix} \tag{9}$$

where L_{ls} and L_{lr} are the per phase winding leakage inductances in the stator and rotor, respectively. L_m is the magnetizing inductance on the stator side. The primed rotor quantities denote values referred to the stator side.

Then the full mathematical description of an induction machine model is presented together with the torque equation

$$T_{em} = \frac{3}{2}\frac{p}{2}\left(\lambda_{ds}i_{qs} - \lambda_{qs}i_{ds}\right) \tag{10}$$

and the rotor speed equation

$$\frac{\mathrm{d}(\omega_r/\omega_b)}{\mathrm{d}t} = \frac{1}{2H}\left(T_{\mathrm{em}} + T_{\mathrm{load}} - T_{\mathrm{damp}}\right)$$

where ω_b is the base value of the angular frequency calculated by $\omega_b = 2\pi f$, f is the supply frequency. p is the number of machine poles. T_{load} is the mechanical torque applied by load, T_{damp} is the damping torque in the direction opposite to the rotor rotation, and H is the inertia constant.

2.2. *Model of induction machine with broken rotor bars*

Broken rotor bars cause asymmetry of the resistance and inductance in rotor phases, which results in asymmetry of the rotating electromagnetic field in the air gap between stator and rotor. Consequently, this will induce frequency harmonics in the stator current. The impact of broken rotor bars can be modelled by unbalancing the rotor resistance, the inductance changes are neglectable due to its insignificance influence compared to the resistance changes [16,20]. For simplicity, for a squirrel-cage rotor, the end-ring contribution is also neglected [16,17]. The stator resistances and inductances stay unchanged.

DOI: 10.1002/etep

The modified rotor resistance in *abc* reference frame is given as follows:

$$\mathbf{r}_r^* = \begin{bmatrix} (r_r + \Delta r_{ra}) & 0 & 0 \\ 0 & (r_r + \Delta r_{rb}) & 0 \\ 0 & 0 & (r_r + \Delta r_{rc}) \end{bmatrix} \tag{11}$$

where Δr_{ra}, Δr_{rb} and Δr_{rc} represent rotor resistance changes in phase a, b and c, respectively, due to broken bar faults. The resistance changes is derived based on the assumption that the broken bars are contiguous, neither the end ring resistance nor the magnetizing current is taken into account, as following. The phase rotor equivalent resistance of a healthy induction motor is given as [16]

$$r_r \approx \frac{(2N_s)^2}{N_b/3} r_b$$

where r_b represents the rotor bar resistances, N_b and N_s are the number of total rotor bars and the equivalent stator winding turns.

When there are n_{bb} broken rotor bars, the increment $\Delta r_{ra,b,c}$ in each phase is obtained as

$$\Delta r_{ra,b,c} = r_r^* - r_r = \frac{(2N_s)^2}{N_b/3 - n_{bb}} r_b - \frac{(2N_s)^2}{N_b/3} r_b = \frac{3n_{bb}}{N_b - 3n_{bb}} r_r \tag{12}$$

To simulate broken rotor bar fault, the rotor resistance matrix in Equation (2) needs to be replaced by the modified rotor resistance matrix $\mathbf{r}_r^*$. Then the Equation (2) needs to be transformed to *qd*0 reference frame [20]. Using the stationary reference frame (setting the *qd*0 rotating speed to zero), the rotor resistance change in Equation (11) can be reorganized in the *qd*0 reference frame as

$$\Delta \mathbf{r}_r^{*qd0} = \begin{bmatrix} r_{r11} & r_{r12} & r_{r13} \\ r_{r21} & r_{r22} & r_{r23} \\ r_{r31} & r_{r32} & r_{r33} \end{bmatrix}$$

where the elements of the matrix are

$$\begin{aligned}
r_{r11} &= \tfrac{1}{3}(\Delta r_{ra} + \Delta r_{rb} + \Delta r_{rc}) + \tfrac{1}{6}(2\Delta r_{ra} - \Delta r_{rb} - \Delta r_{rc})\cos(2\theta_r) + \tfrac{\sqrt{3}}{6}(\Delta r_{rb} - \Delta r_{rc})\sin(2\theta_r) \\
r_{r12} &= -\tfrac{1}{6}(2\Delta r_{ra} - \Delta r_{rb} - \Delta r_{rc})\sin(2\theta_r) + \tfrac{\sqrt{3}}{6}(\Delta r_{rb} - \Delta r_{rc})\cos(2\theta_r) \\
r_{r13} &= \tfrac{1}{3}(2\Delta r_{ra} - \Delta r_{rb} - \Delta r_{rc})\cos(\theta_r) - \tfrac{\sqrt{3}}{3}(\Delta r_{rb} - \Delta r_{rc})\sin(\theta_r) \\
r_{r21} &= r_{r12} \\
r_{r22} &= \tfrac{1}{3}(\Delta r_{ra} + \Delta r_{rb} + \Delta r_{rc}) - \tfrac{1}{6}(2\Delta r_{ra} - \Delta r_{rb} - \Delta r_{rc})\cos(2\theta_r) + \tfrac{\sqrt{3}}{6}(\Delta r_{rb} - \Delta r_{rc})\sin(2\theta_r) \\
r_{r23} &= -\tfrac{1}{3}(2\Delta r_{ra} - \Delta r_{rb} - \Delta r_{rc})\sin(\theta_r) - \tfrac{\sqrt{3}}{3}(\Delta r_{ra} - \Delta r_{rc})\cos(\theta_r) \\
r_{r31} &= \tfrac{1}{2} r_{r13} \\
r_{r32} &= \tfrac{1}{2} r_{r23} \\
r_{r33} &= \tfrac{1}{3}(\Delta r_{ra} + \Delta r_{rb} + \Delta r_{rc})
\end{aligned}$$

2.3. Model of induction machine with shorted stator windings

The shorted stator winding fault in an induction machine can be modelled in a similar manner with the broken rotor bar fault. In the ideal situation, all stator parameters are considered to be identical in three phases. When a short circuit between stator turns occurs in a given phase, the corresponding number of windings will decrease [18]. Here, both the changes of stator resistance and inductance due to short circuit have to be taken into account.

An approximate relationship between the portion of short circuit and the change of winding inductance in stator is that to consider the leakage inductance to be proportional to squared turns number [21]. While the rotor inductances $\mathbf{L}_{rr}^{abc}$ remain unchanged ($\mathbf{r}_r$ should be replaced by $\mathbf{r}_r^*$ if rotor faults present), the stator electrical parameters $\mathbf{r}_s$, $\mathbf{L}_{ss}^{abc}$, and the mutual inductances between the stator and rotor ($\mathbf{L}_{sr}^{abc}$ and $\mathbf{L}_{rs}^{abc}$), are directly affected.

Let g_{sa}, g_{sb} and g_{sc} be the percentage of the remaining un-shorted stator windings in stator phase a, b and c, respectively. The modified stator resistance matrix $\mathbf{r}_s^*$ has a similar structure with the modified rotor resistance matrix $\mathbf{r}_r^*$ in Equation (11) for broken rotor bar fault.

DOI: 10.1002/etep

Here, the modified stator self inductance matrix $\mathbf{L}_{ss}^{*abc}$ is given as [18]

$$\mathbf{L}_{ss}^{*abc} = \begin{bmatrix} g_{sa}^2(L_{ls}+L_{ss}) & g_{sa}g_{sb}L_{sm} & g_{sa}g_{sc}L_{sm} \\ g_{sa}g_{sb}L_{sm} & g_{sb}^2(L_{ls}+L_{ss}) & g_{sb}g_{sc}L_{sm} \\ g_{sa}g_{sc}L_{sm} & g_{sb}g_{sc}L_{sm} & g_{sc}^2(L_{ls}+L_{ss}) \end{bmatrix} \tag{13}$$

The modified stator-to-rotor mutual inductance matrix $\mathbf{L}_{sr}^{*abc}$ is expressed as

$$\mathbf{L}_{sr}^{*abc} = L_{sr}\begin{bmatrix} g_{sa}\cos\theta_r & g_{sa}\cos\left(\theta_r+\frac{2\pi}{3}\right) & g_{sa}\cos\left(\theta_r-\frac{2\pi}{3}\right) \\ g_{sb}\cos\left(\theta_r-\frac{2\pi}{3}\right) & g_{sb}\cos\theta_r & g_{sb}\cos\left(\theta_r+\frac{2\pi}{3}\right) \\ g_{sc}\cos\left(\theta_r+\frac{2\pi}{3}\right) & g_{sc}\cos\left(\theta_r-\frac{2\pi}{3}\right) & g_{sc}\cos\theta_r \end{bmatrix} \tag{14}$$

and the modified rotor-to-stator mutual inductance matrix $\mathbf{L}_{rs}^{*abc}$ can be easily obtained as

$$\mathbf{L}_{rs}^{*abc} = \left[\mathbf{L}_{sr}^{*abc}\right]^T$$

In these matrices L_{ss} and L_{rr} are the self-inductances in the stator and rotor, respectively. L_{sm} and L_{rm} are the mutual inductance between the stator windings and that between the rotor windings, respectively. L_{sr} is the peak value of the stator-to-rotor mutual inductance, and the superscript T denotes the transpose of the matrix.

In the same manner, these modified resistance and inductance matrices are used as substitutes for their original ones in Equations (1) and (2). Then the *qd*0 reference frame transformation needs to be performed to these equations. By doing so and assuming that the short circuit occurs only in phase *a* of the stator for simplicity, the resistance matrix of stator with shorted turns in the *qd*0 reference frame can be derived as

$$\mathbf{r}_s^{*qd0} = r_s\begin{bmatrix} r_{s11} & 0 & r_{s13} \\ 0 & r_{s22} & 0 \\ r_{s31} & 0 & r_{s33} \end{bmatrix}$$

where the non-zero elements of the matrix are

$$r_{s11} = \frac{1}{3}(2g_{as}+1),\ r_{s13} = \frac{2}{3}(g_{as}-1),\ r_{s22} = 1,\ r_{s31} = \frac{1}{3}(g_{as}-1),\ \text{and}\ r_{s33} = \frac{1}{3}(g_{as}+1)$$

The stator and rotor flux linkage matrices in Equation (9) can be modified as

$$\begin{bmatrix} \lambda_s^{*qd0} \\ \lambda_r^{*'qd0} \end{bmatrix} = \begin{bmatrix} L_{11} & 0 & L_{13} & L_{14} & 0 & 0 \\ 0 & L_{22} & 0 & 0 & L_{25} & 0 \\ L_{31} & 0 & L_{33} & L_{34} & 0 & 0 \\ L_{41} & 0 & L_{43} & L_{44} & 0 & 0 \\ 0 & L_{52} & 0 & 0 & L_{55} & 0 \\ 0 & 0 & 0 & 0 & 0 & L_{66} \end{bmatrix} \begin{bmatrix} \mathbf{i}_s^{qd0} \\ \mathbf{i}'^{qd0}_r \end{bmatrix} \tag{15}$$

where the elements of the matrix are

$$\begin{aligned} L_{11} &= \tfrac{1}{3}\left(2g_{sa}^2+1\right)L_{ls} + \tfrac{1}{9}(2g_{sa}+1)^2L_m \\ L_{13} &= \tfrac{2}{3}\left(g_{sa}^2-1\right)L_{ls} + \tfrac{2}{9}\left(2g_{sa}^2-g_{sa}-1\right)L_m \\ L_{14} &= L_{41} = \tfrac{1}{3}(2g_{sa}+1)L_m \\ L_{22} &= L_{ls}+L_m \\ L_{25} &= L_{52} = L_m \\ L_{31} &= \tfrac{1}{3}\left(g_{sa}^2-1\right)L_{ls} + \tfrac{1}{9}\left(2g_{sa}^2-g_{sa}-1\right)L_m \\ L_{33} &= \tfrac{1}{3}\left(g_{sa}^2+2\right)L_{ls} + \tfrac{2}{9}\left(g_{sa}^2-2g_{sa}-1\right)L_m \\ L_{34} &= \tfrac{1}{3}(g_{sa}-1)L_m \\ L_{43} &= 2L_{34} \\ L_{44} &= L_{55} = L'_{lr}+L_m \\ L_{66} &= L'_{lr} \end{aligned}$$

DOI: 10.1002/etep

3. THE IMPLEMENTATION OF THE MODEL IN MATLAB/SIMULINK

Having derived the induction machine differential equations system, in this section, the implementation of the model in Matlab/Simulink is detailed. Normally, a healthy induction machine model is easy to achieve [19]. When substitute the balanced electrical parameters of a healthy induction machine with their unbalanced modifications, which represent the rotor and stator faults, the reference frame transformation turns quite complicated. Therefore, a systemic approach is needed to better construct the model.

Machine parameters are always determined in terms of the flux linkage per second, ψ, and the reactance, x, instead of λ and L in experiments. These quantities have the following relationship: $\psi = \omega_b \lambda$ and $x = \omega_b L$. To use Simulink, the stator and rotor voltage differential equations in the $qd0$ reference frame need to be rewritten as self-referencing integral functions of the flux linkages, as follows:

$$\begin{aligned} \psi_s^{*qd0} &= \omega_b \int \left\{ \mathbf{u}_s^{qd0} - \mathbf{r}_s^{*qd0} \mathbf{i}_s^{qd0} \right\} \mathrm{d}t \\ \psi_r^{*qd0} &= \omega_b \int \left\{ \mathbf{u}_r^{qd0} - \mathbf{r}_r^{*'qd0} \mathbf{i}_r^{qd0} \right\} \mathrm{d}t \end{aligned} \tag{16}$$

The stator and rotor current in the $qd0$ reference frame are calculated by using inverted Equation (15), and then feed back to Equation (16).

In Simulink, all functions are implemented in function blocks. There are seven main modules in the model: the *abc*-$qd0$ conversion module, the unit vector calculation module, the q, d, 0 quantities calculation modules, the torque/speed module and the $qd0$-*abc* conversion module. The content of these modules are illustrated in Figures 1–7.

Figure 1 shows the content of *abc*–$qd0$ conversion module. Voltage quantities in *abc* reference frame are converted to the $qd0$ reference frame. The function inserted in this module is the transformation Equation (5). The $qd0$–*abc* module which transforms the stator currents from $qd0$ back to *abc* reference frame has an identical structure with the one shown in Figure 1. However, the functions inserted in the blocks are the inverse of the matrix in Equation (5). The unit vector module is presented in Figure 2. It has

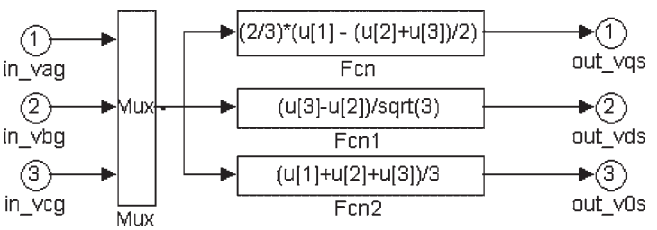

Figure 1. Block diagram of the *abc*-$qd0$ transformation module in Simulink.

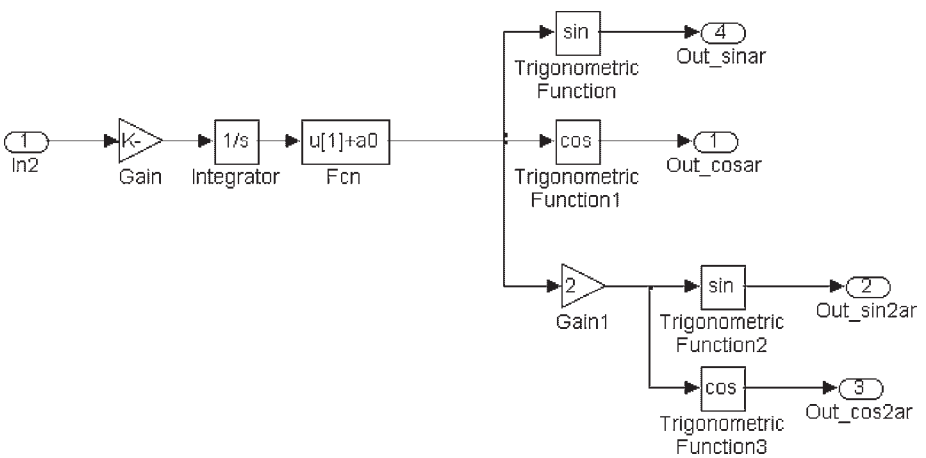

Figure 2. Block diagram of the unit vector module in Simulink.

DOI: 10.1002/etep

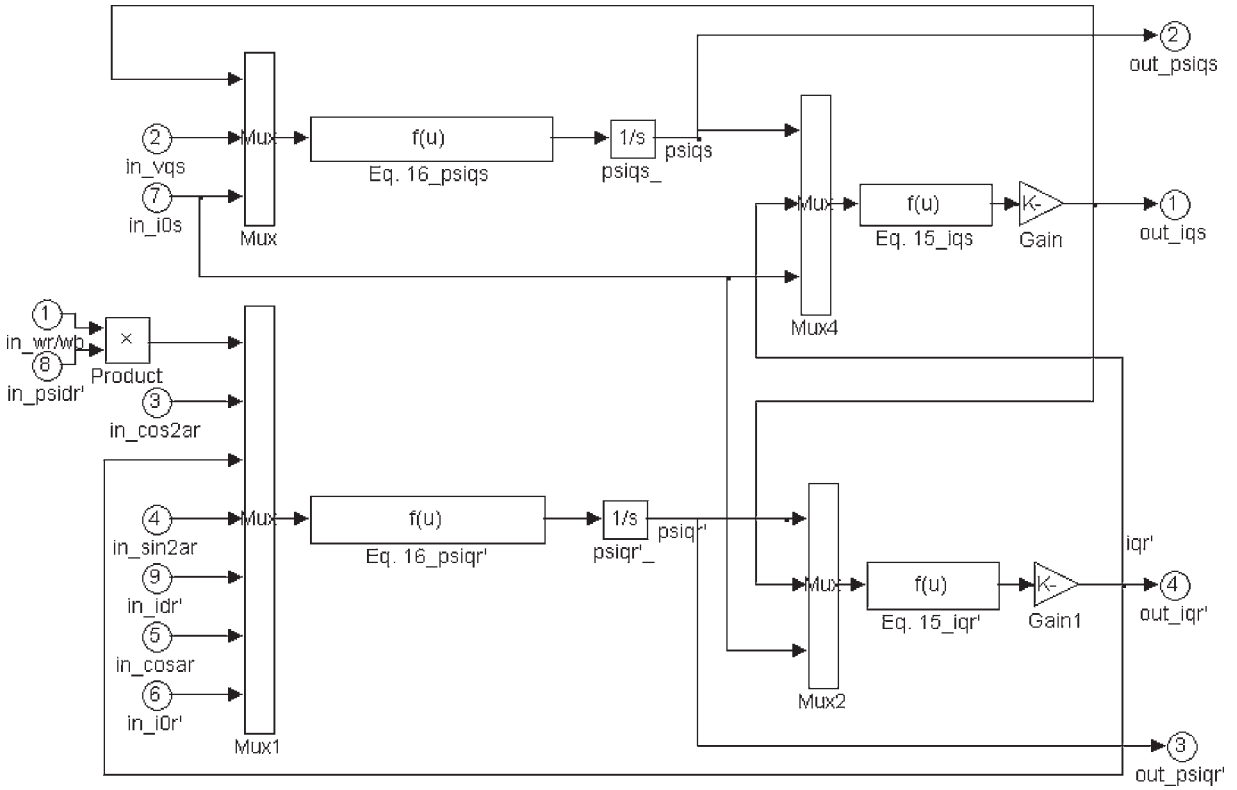

Figure 3. Block of the *q*-axis module in Simulink.

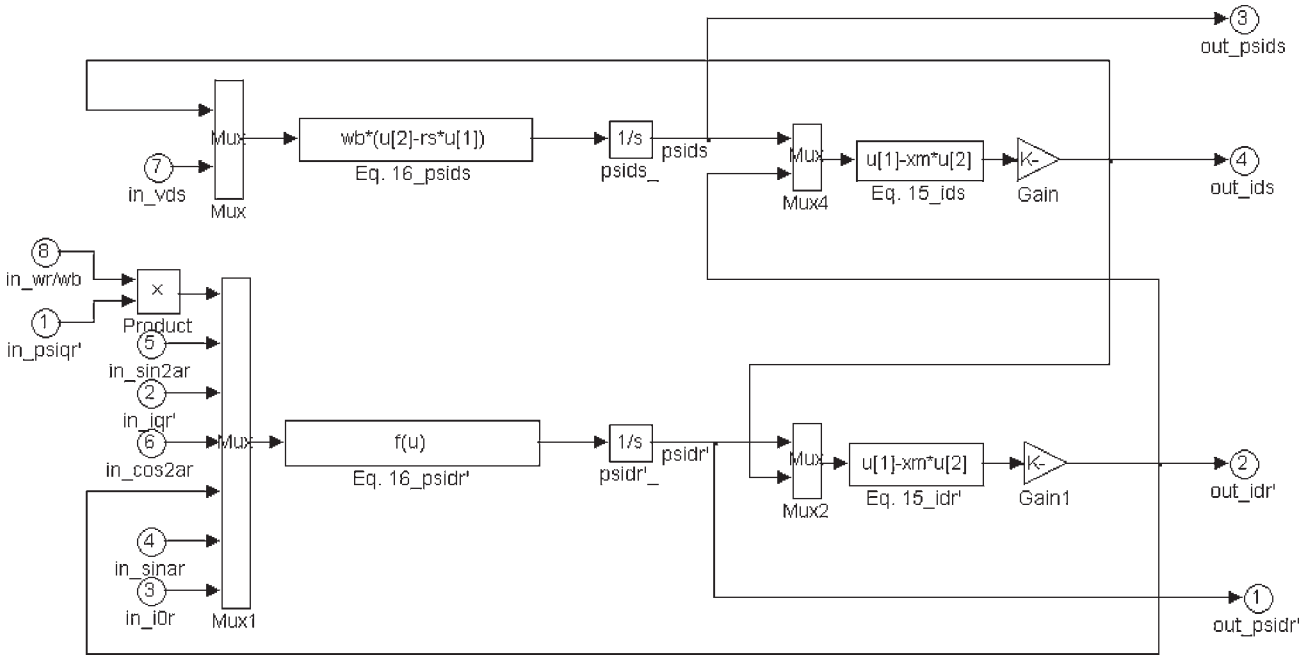

Figure 4. Block diagram of the d-axis module in Simulink.

DOI: 10.1002/etep

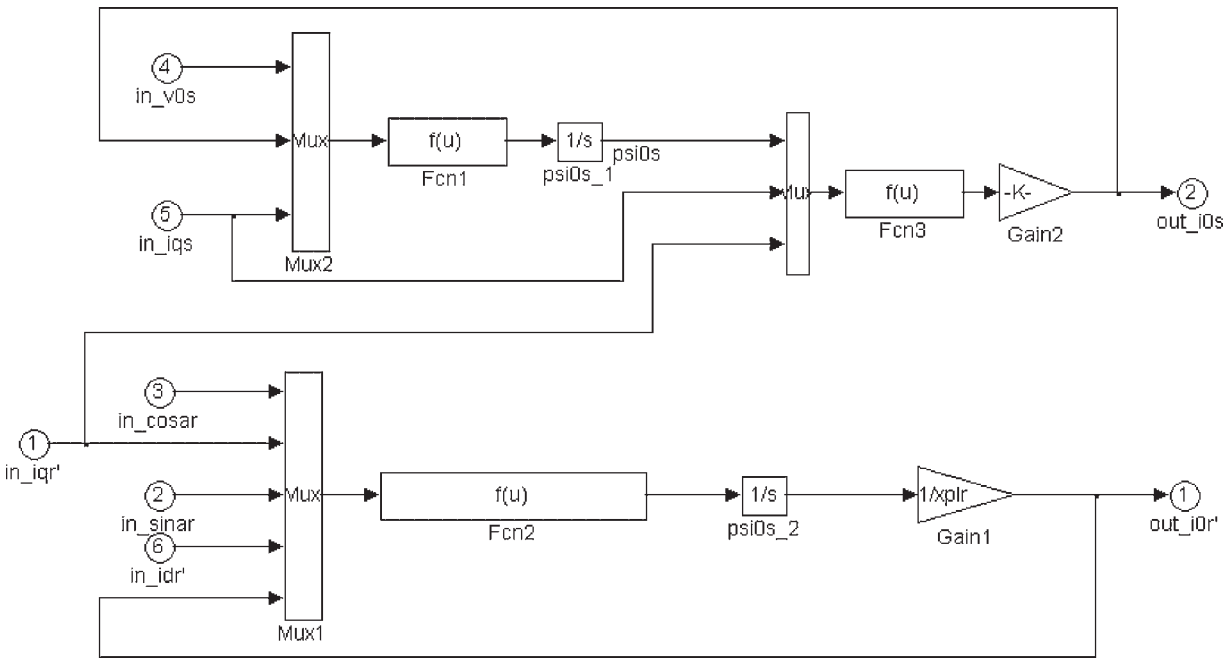

Figure 5. Block diagram of the zero sequence module in Simulink.

the rotor angular speed as input and calculates the $\sin(\theta_r)$, $\sin(2\theta_r)$, $\cos(\theta_r)$ and $\cos(2\theta_r)$, which are the inputs for determining stator and rotor variables in the $qd0$ sequence. The q, d and 0 sequence modules are the core components which calculate the flux linkages, currents and voltages in the $qd0$ reference frame. The content of these three modules are given in Equations (15) and (16). The arrangements of the equations are shown in Figures 3–5. The torque/speed module calculates the output torque and the rotor angular speed, as illustrated in Figure 6. The overall view of the dynamic induction motor model in Simulink is shown in Figure 7.

To conduct the simulation, the Simulink model needs to be initialized previously to assign values to all machine and operation condition parameters. The inputs to the model are three-phase voltage and load torque. Both the number of broken rotor bars and the percentage of shorted stator windings can be easily changed to any desired values.

4. EXPERIMENT SETUP FOR MODEL VALIDATION

In order to validate the model, a laboratory experiment is conducted. A commercial 5.5 kW, 50 Hz, 4 poles induction machine, which has a standard cast aluminium squirrel cage rotor with 32 rotor slots, is used in the test. A separately excited DC generator is coupled

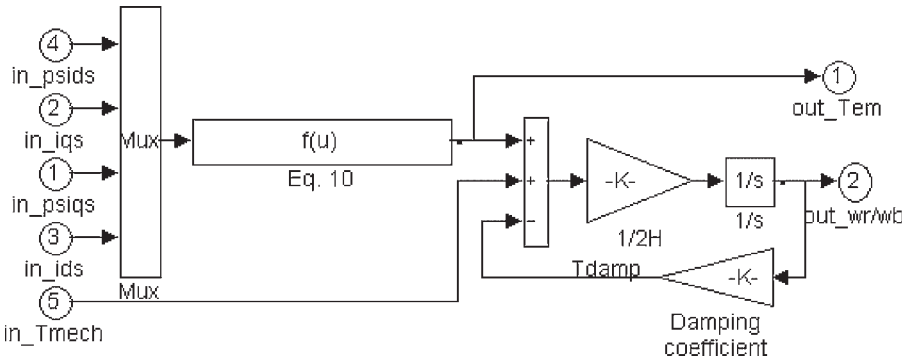

Figure 6. Block diagram of the torque/rotor module in Simulink.

DOI: 10.1002/etep

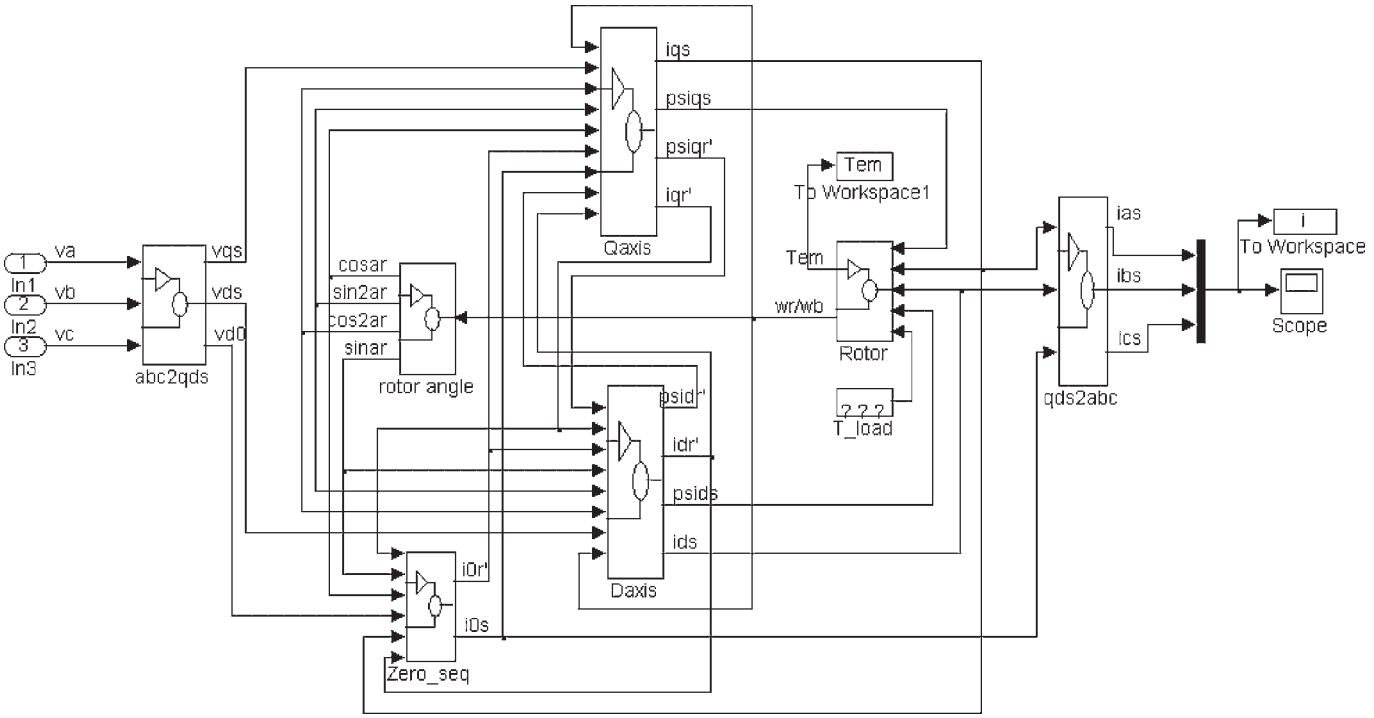

Figure 7. Overall view of the dynamic induction motor model in Simulink.

via a belt as load, and is loaded by using a variable resistance bank. The broken rotor bar fault is constructed by cutting holes through the rotor bars at the joints with the end ring using a fine milling cutter.

The stator current is sensed by a Hall-Effect clamp probe, passed through an anti-aliasing filter, which is an 8th order Butterworth filter, and finally sampled by an A/D converter. A custom written LabVIEW data acquisition system is used for data acquisition [22].

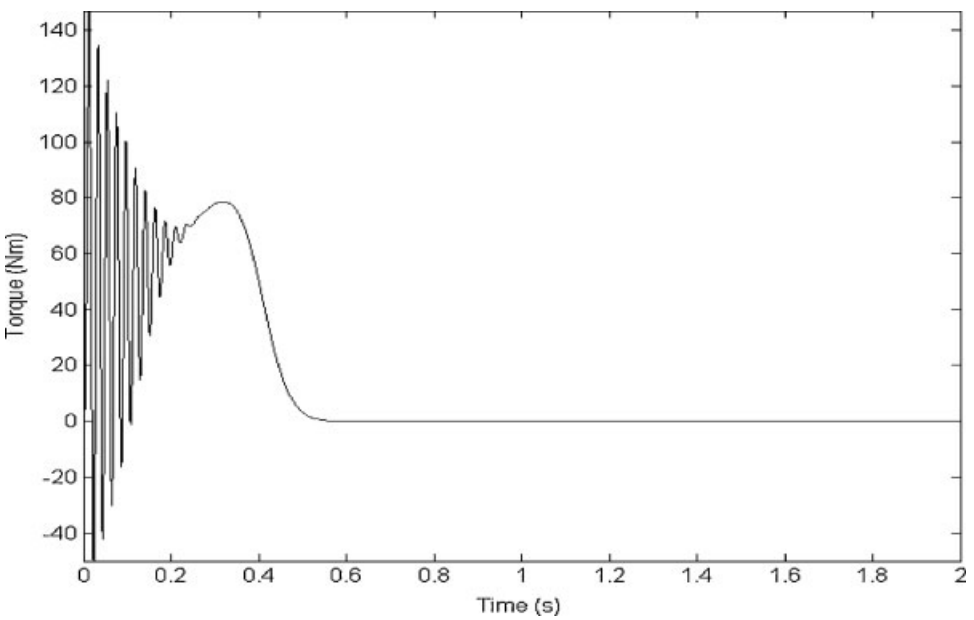

Figure 8. Simulated motor starting torque.

DOI: 10.1002/etep

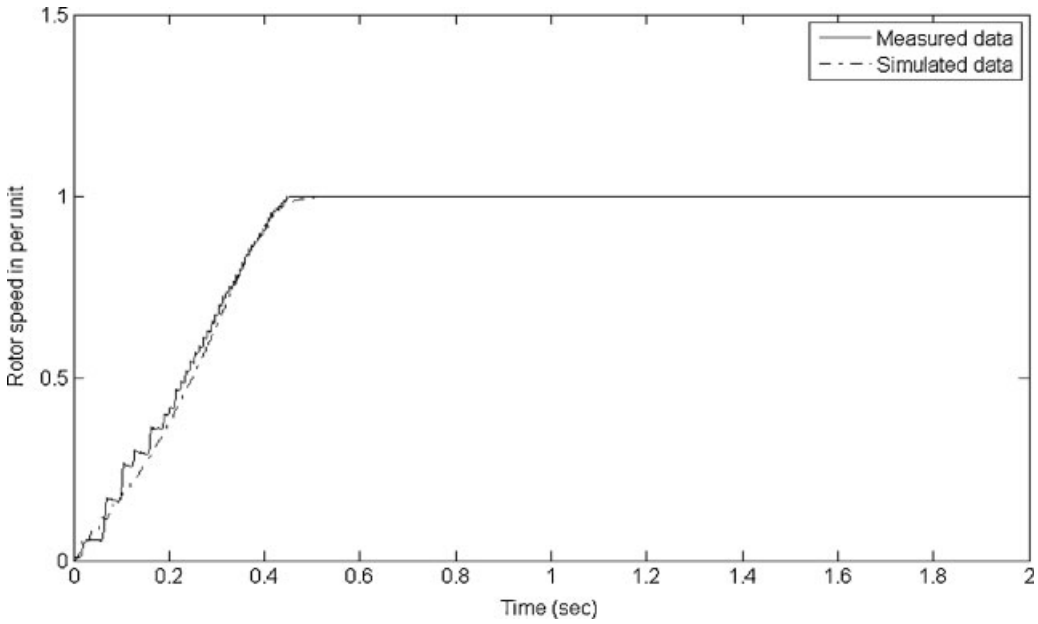

Figure 9. Comparison of the simulated and measured rotor speed.

Based on the described induction motor model and machine parameters that are measured from a real three-phase, 4-pole, 5.5 kW induction motor, simulations in Matlab/Simulink have been conducted. Figure 8 presents the output torque curve obtained from the simulation. The simulated rotor speed and stator current curves are plotted and compared with the measured signal in Figures 9 and 10, respectively. In Figure 9, a considerable agreement between simulated and measured rotor speed curves can be observed. The simulated stator current is plotted with a small phase shift in respect to the measured data for comparison in Figure 10.

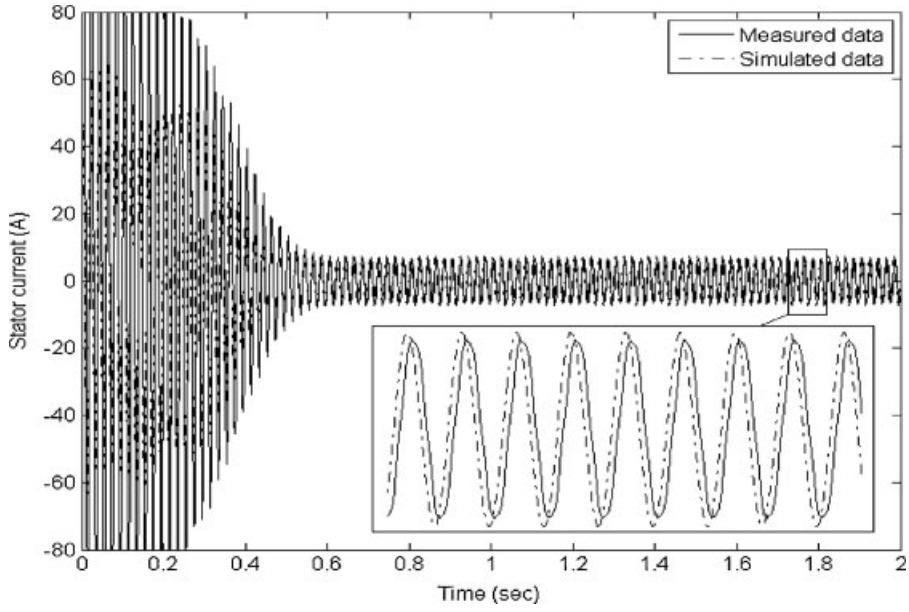

Figure 10. Comparison of the simulated and measured stator current.

DOI: 10.1002/etep

Magnitude difference exists in the transient state but both the simulated and measured currents enter the steady state at the same time. Also, zoomed in view of the comparison in steady state is presented as only the current in steady state is related to the methods of broken rotor bar diagnostics that presented in the paper.

5. TESTING FAULT DIAGNOSTICS METHODS USING THE SIMULATION TOOL

5.1. Broken rotor bar detection using high-resolution spectral analysis and comparison with DFT

It is well established that broken rotor bars in an induction machine can be detected by investigating the presence of side band frequency components $(1 \pm 2s)f$ in the stator current spectrum [1,2], where s is the machine slip. The proposed model can accurately simulate this phenomenon. Figure 11 presents the spectrum of the simulated stator current of the previously mentioned induction machine in healthy condition. Figure 12 shows the current spectral lines when the number of broken rotor bars varies from 1 to 5, while Figure 13 illustrates the movement of the sideband frequencies along with the load condition. In the simulated stator current data, sideband frequencies are clearly displayed, their amplitude increase when the more broken rotor bars occur and their positions move towards the supply frequency when the load is lighter.

The sideband frequencies have such a property that they are two small peaks present in the vicinity of a large peak. Besides, in practice they can be moving due to the changing of the machine load, and can be very close to the supply frequency due to the light load conditions. Traditionally, DFT is used for analysis of stator current in frequency domain. However, to maintain a high resolution, DFT requires a long data window. This is worsen if the load is light, and is troublesome if the sideband frequencies are moving. Therefore, trade-off among leakage suppression, resolution and stability is hard to be fulfilled when using DFT.

In this paper, a high-resolution spectral analysis technique called Prony Analysis (PA) [23] is proposed to replace DFT for the diagnostic of broken rotor bars. The main motivation is that the PA can be successfully implemented with short data window while keeping high resolution in frequency domain. The method is a parametric spectral analysis technique for modelling a uniformly sampled signal *y(n)* using a linear combination of q damped exponential functions [24]

$$y(n) = \sum_{k=1}^{q} A_k \exp[(\alpha_k + j2\pi f_k)(n-1)T_s + j\theta_k] \tag{17}$$

for $n = 1,2,\ldots,N$

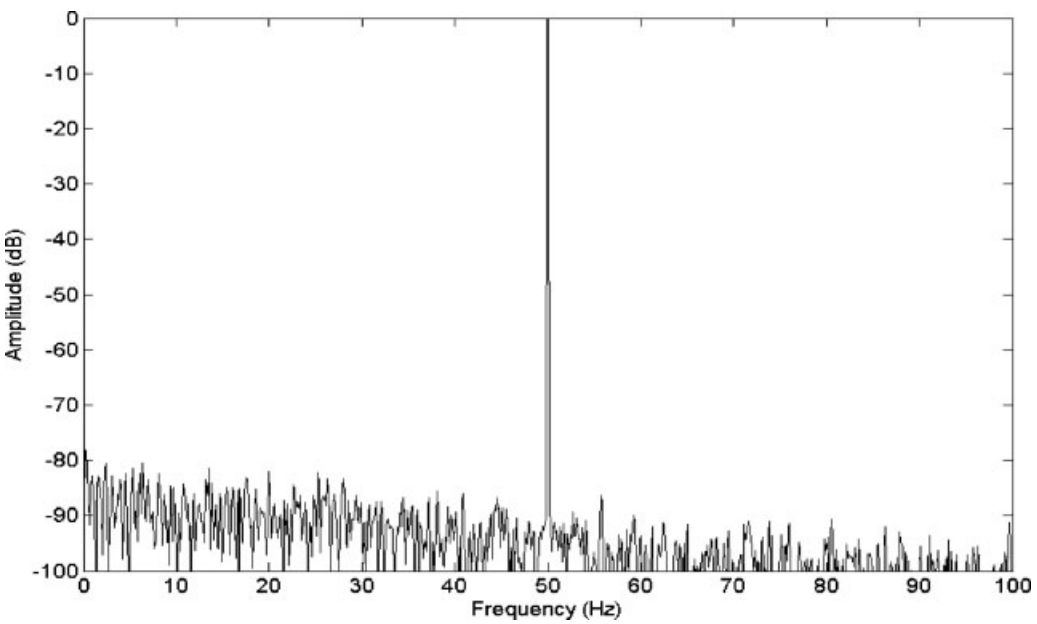

Figure 11. Frequency spectrum of the simulated stator current of a 5.5 kW induction machine with no broken rotor bars.

DOI: 10.1002/etep

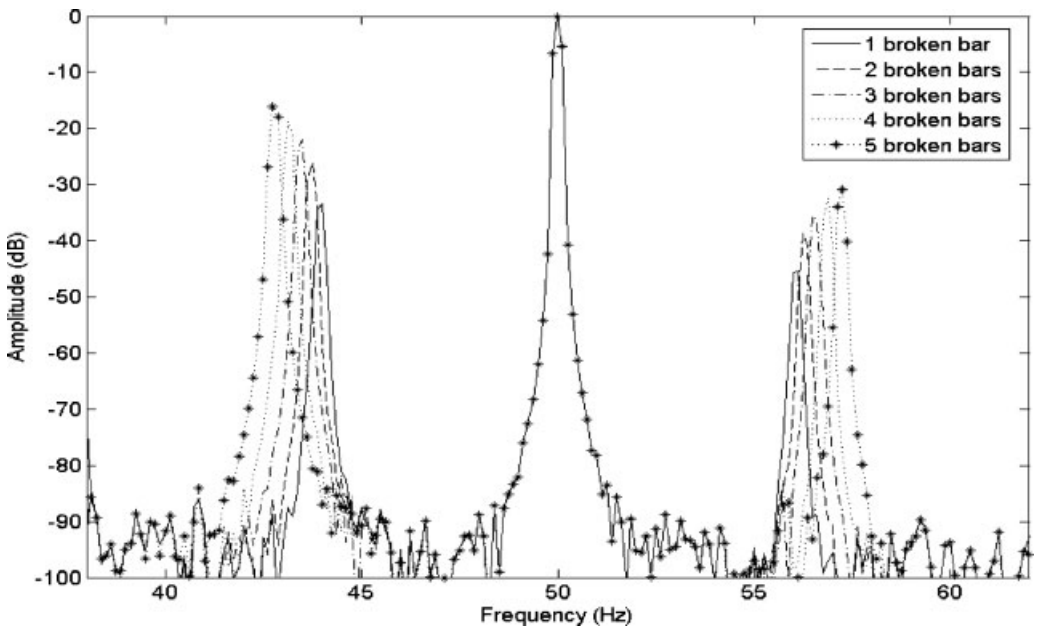

Figure 12. Frequency spectra of the simulated stator current of a 5.5 kW induction machine with 1, 2, 3, 4 and 5 broken rotor bars.

where A_k is the amplitude of the complex exponential, α_k is the damping factor in seconds^{-1}, f_k is the sinusoidal frequency in Hz, θ_k is the initial phase in radians and T_s is the sample interval in seconds.

Since only real signals are considered, the signal poles $\exp(\alpha_k + j2\pi f_k)$ must appear in complex conjugate pairs.

The key of the Prony's method is in the fact that a linear combination of damped exponentials is the solution to a homogeneous linear difference equation with constant coefficients. By expressing Equation (17) in a concise way

$$y(n) = \sum_{k=1}^{q} h_k z_k^{n-1}$$

where $h_k = A_k \exp(j\theta_k)$ and $z_k = \exp[(\alpha_k + j2\pi f_k)T_s]$. The use of this method can be then summarized into three steps [17]:

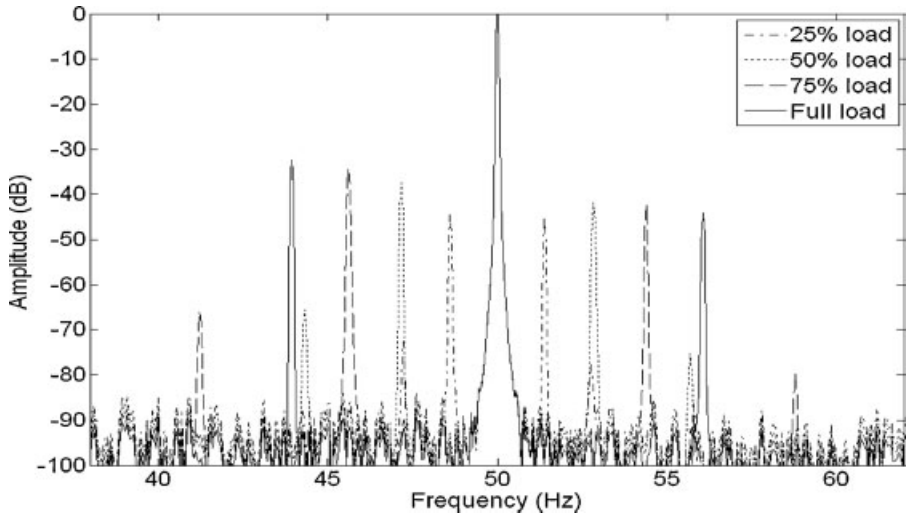

Figure 13. Frequency spectra of the simulated stator current of a 5.5 kW induction machine with 1 broken bar operating under 25, 50, 75 and 100% of full load.

DOI: 10.1002/etep

Step 1 Determine the linear prediction parameters that fit the observed data.
Step 2 Find roots of characteristic polynomial formed from the linear prediction coefficients. The estimates of damping and sinusoidal frequencies of each of the exponential terms can be determined consequently.
Step 3 Solve the original set of linear equation to yield the estimates of the exponential amplitude and sinusoidal initial phase.

In practice, the Iteratively Reweighted Least Squares (IRLS) Prony method can efficiently attenuate the effect of noise by using a weighting matrix to take into account the previous signal error [25]. When the signal is corrupted with noise, Equation (17) will then become

$$y(n) = \sum_{k=1}^{q} h_k z_k^{n-1} + \varepsilon(n)$$

where $\varepsilon(n)$ represents the exponential prediction approximation error. The first step of PA is then modified as

$$\mathbf{Ya} + \mathbf{b} + \mathbf{D}(\mathbf{a})\varepsilon = 0,$$

where $\mathbf{Y}$ is the data matrix from $y(1)$ to $y(N-1)$ with Toeplitz structure, $\mathbf{b}$ is the column vectors of data points from $y(q+1)$ to $y(N)$, $\mathbf{a}$ is column vectors of the q difference equation coefficients and $\mathbf{D}$ is the error weighting matrix

$$\mathbf{D} = \begin{bmatrix} a_q & a_{q-1} & \cdots & a_1 & 1 & 0 & \cdots & 0 \\ 0 & a_q & a_{q-1} & \cdots & a_1 & 1 & \cdots & 0 \\ \vdots & \ddots & \ddots & \ddots & \cdots & \ddots & \ddots & \vdots \\ 0 & \cdots & 0 & a_q & a_{q-1} & \cdots & a_1 & 1 \end{bmatrix}$$

Prefiltering is also used to improve the performance of PA dealing with noisy signal [26]. A detailed implementation of IRLS Prony can be found in Reference [27].

Figure 14 shows the spectrum calculated with DFT of a simulated stator current from a 5.5 kW induction machine with one broken bars operating under only 25% of the rated load. The sample frequency is 1000 Hz with a data window length of 3000 samples, in order to achieve enough resolution to observe broken bar sidebands. Signal data is processed by a Hanning window before applying

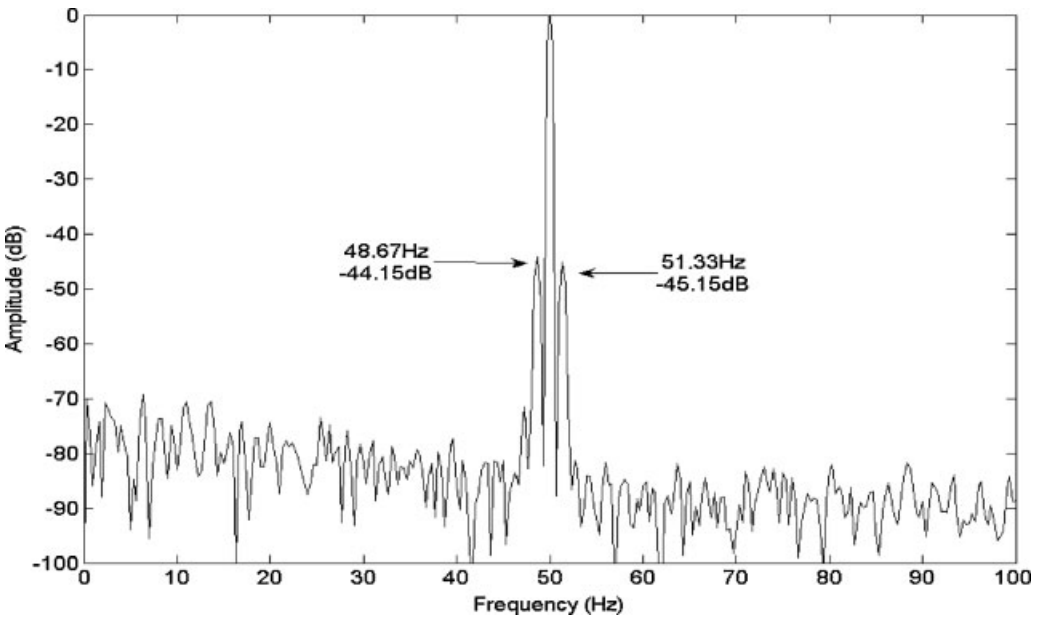

Figure 14. Frequency spectrum of the stator current of a 5.5 kW induction machine with one broken bar operating under 25% of full load. Sampling frequency: 1000 Hz; window length: 3000 samples.

DOI: 10.1002/etep

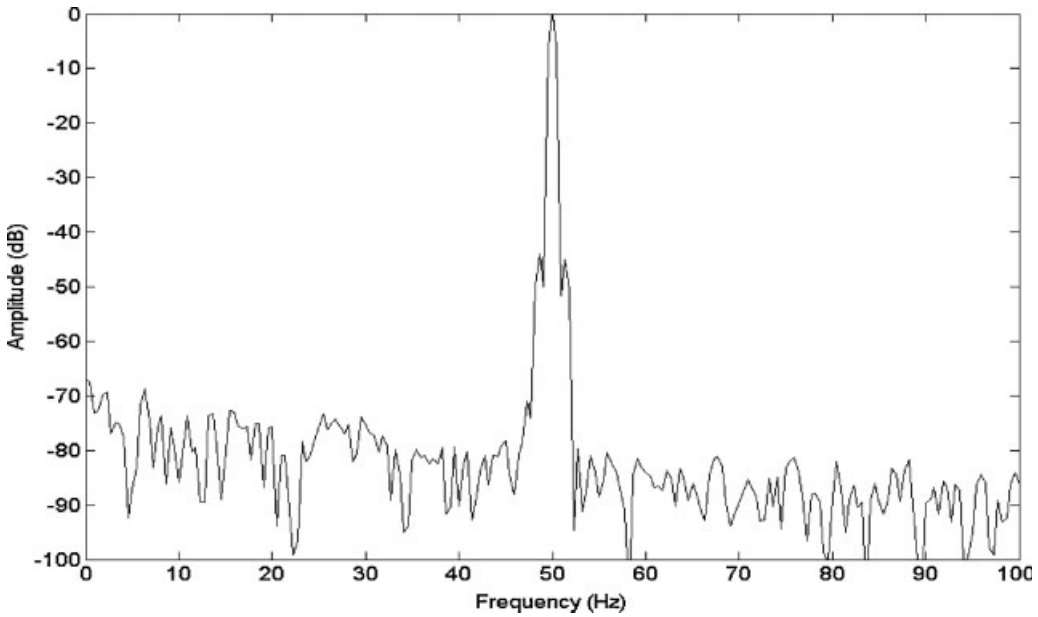

Figure 15. Frequency spectrum of the stator current of a 5.5 kW induction machine with one broken bar operating under 25% of full load. Sampling frequency: 1000 Hz; window length: 2200 samples.

the FFT algorithm to decrease the spectral leakage effect and to shape the signal spectrum. From the spectrum in Figure 14, the two broken bar sidebands can still be seen very close to the 50 Hz. However, if a shorter data window, for example, that of 2200 samples is used, the two sideband frequencies will merge into the supply frequency and cannot be distinguished. This is revealed in Figure 15. Thus, DFT with shorter data windows is not able to maintain a resolution high enough to observe the sideband frequencies. When the load is lighter, even longer window is required.

However, the result obtained by the IRLS PA with very short data window in Table I show that the two-sideband frequencies are clearly estimated. In this case, the sampling frequency is still 1000 Hz but only 100 data samples are used. If the induction machine is operating under full rated load, the slip will be larger and the two-sideband frequencies are more apart from the supply frequency. In this case, PA can be implemented using a considerably shorter data window, as the result shown in Table II. In this case, only 50 samples are used.

Table I. PA result of the same signal used in Figure 15. Sampling frequency: 1000 Hz; window length: 100 samples.

Frequency (Hz)			
True value	48.6136	50.0000	51.3864
PA result	48.4876	50.0091	51.1640
Amplitude (dB)			
PA result	−43.3138	0	−45.6439

Table II. PA result of the stator current of a 5.5 kW induction machine with one broken bar operating under full load. Sampling frequency: 1000 Hz; window length: 50 samples.

Frequency (Hz)			
True value	43.9431	50.0000	56.0569
PA result	43.9650	49.9998	56.0570
Amplitude (dB)			
PA result	−31.2345	0	−43.1416

DOI: 10.1002/etep

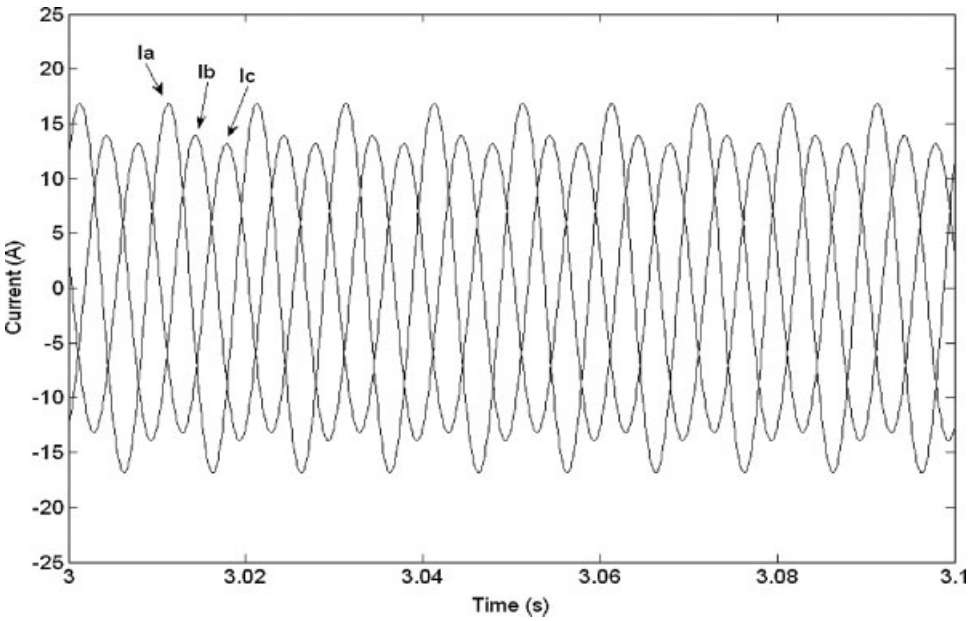

Figure 16. Simulated three-phase stator current of an induction machine with 4% shorted turns in phase *a*.

5.2. Simulation and diagnostics of shorted Stator Wingdings

The model presented in the paper can not only simulate the broken rotor bar conditions, but also the shorted stator winding faults in an induction machine.

Stator winding faults imbalance the stator phase resistance and inductance. In the simulation, 4% of the windings in phase *a* of the stator are shorted. An increase of the current amplitude in phase *a* can be noticed clearly in Figure 16. The pattern of the current

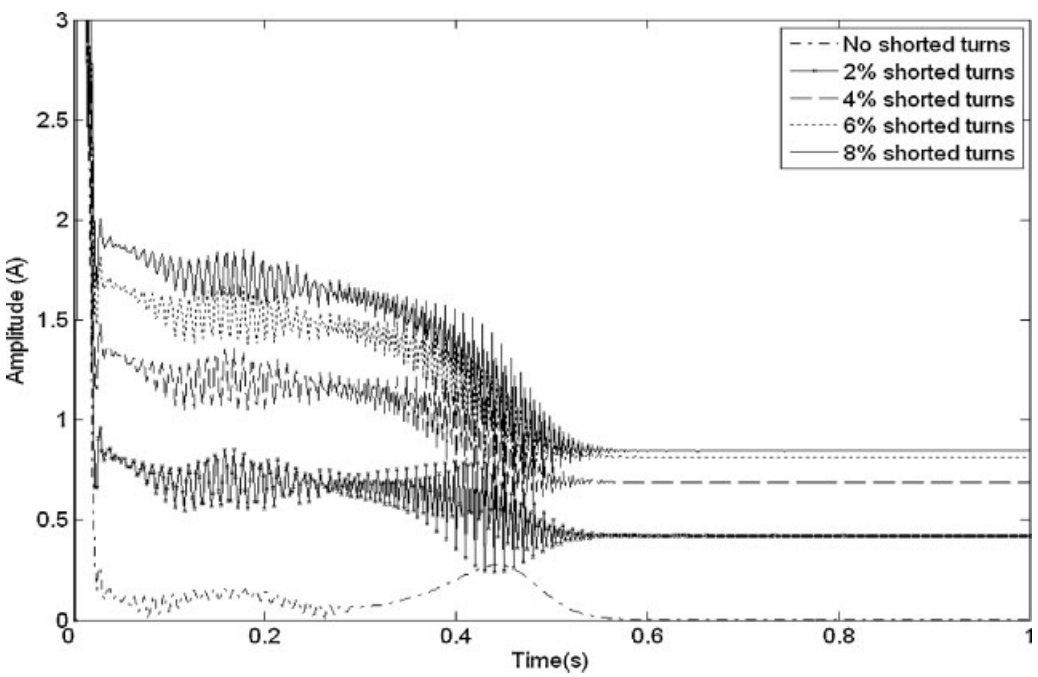

Figure 17. Simulated negative sequence currents from stand still to full speed of an induction machine with different degrees of shorted turns.

DOI: 10.1002/etep

anomaly is exactly the same with that reported in Reference [18]. The amplitude of short current will increase when the percentage of shorted windings is higher.

The occurrence of negative sequence current is identified when shorted stator windings are present [21,28]. Figure 17 shows the negative sequence currents of an induction machine with different percentages of shorted stator windings during the start up until steady state. There is no negative sequence current in steady state when the motor stator winding is in a healthy condition, while the

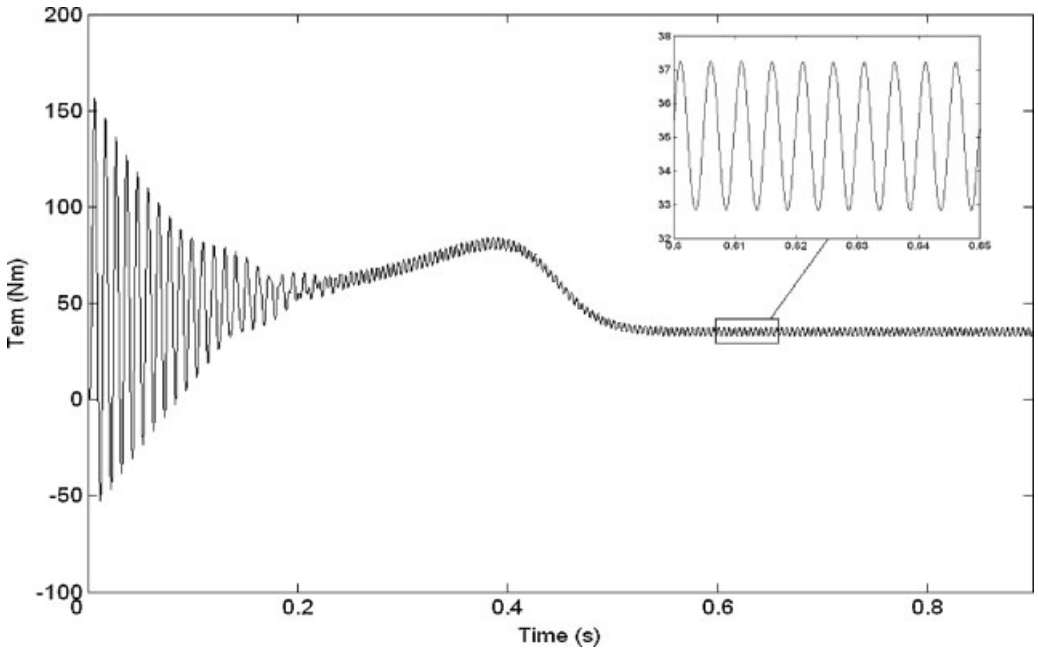

Figure 18. Simulated torque curve from stand still to full speed of an induction machine with 4% shorted turns in phase *a*.

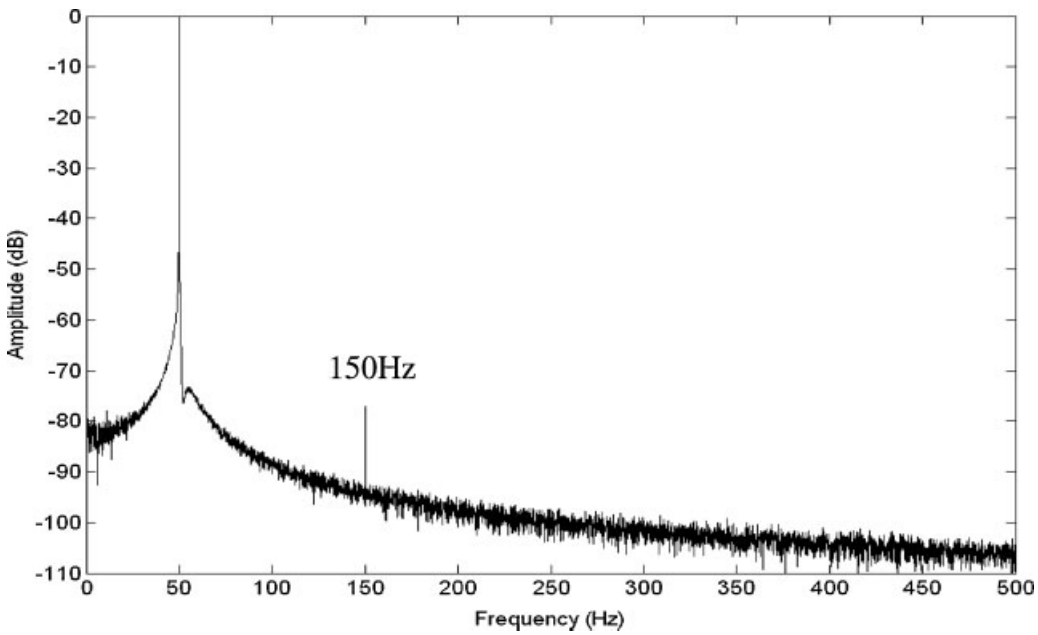

Figure 19. Frequency spectrum of simulated stator current of an induction machine with 4% shorted turns in phase *a*.

DOI: 10.1002/etep

amplitude of the negative sequence current rises if the percentage of shorted windings increases. Figure 18 presents the torque of this motor. The torque pulsation caused by shorted stator windings is clearly seen in the simulation and it is comparable with those previously observed in References [28] and [29].

Another stator winding fault indicator is the harmonic frequency component at $3f$ Hz in the stator current [3,30], where f is the fundamental frequency. This is explained as the speed ripple effect [30]. The rise of this frequency component can be observed from Figure 19.

6. CONCLUSION

Broken rotor bars and shorted stator windings are common faults in induction machines. In this paper, an induction machine model for testing fault diagnostic techniques has been presented. This model is based on the Coupled Circuit Approach and is achieved in Matlab/Simulink. It can simulate both the broken rotor bar and the shorted stator winding faults.

A fault in either the rotor or stator of an induction machine adds anomalies to the symmetry of electrical quantities, which are originally designed to be symmetric. To simulate broken rotor bar faults, changes in rotor phase resistance are introduced, while to simulate shorted stator winding fault, both the changes in stator phase resistance and inductance have to be taken into account. These changes are made in *abc* reference frame initially, and then transformed to the *qd*0 reference frame for modelling. Details of modelling faulty induction machines in Simulink are presented in the paper with diagrams of each function module.

Simulation results of both rotor and stator fault conditions show same properties with that have been reported by other researchers. These features can be used as fault indicators for motor fault diagnostics. The number of broken rotor bars and the percentage of shorted stator windings can be easily changed in the simulation model to any values. The simulation results can be used to study fault diagnostic techniques.

Testing result of using IRLS PA in broken rotor bar detection is presented. The results are compared with the traditional approach based on DFT. PA is a high-resolution spectral analysis technique and it is illustrated to outperform DFT in terms of maintaining high resolution in frequency domain while using a considerably shorter data window. This allows PA to overcome problems that DFT encounters in situations such as changing or light load conditions.

7. LIST OF SYMBOLS

$\mathbf{a}$	column vectors of difference equation coefficients
A_k	amplitude of the complex exponentials
$\mathbf{b}$	column vectors of data points from $y(q+1)$ to $y(N)$
$\mathbf{D}$	error weighting matrix
f	fundamental frequency
f_k	sinusoidal frequencies
$g_{sa,b,c}$	percentage of the remaining un-shorted windings in stator phase a, b or c
H	inertia constant
$\mathbf{i}_{s,r}^{abc}$	column vectors of three-phase stator or current currents in *abc* reference frame
$\mathbf{i}_{s,r}^{qd0}$	column vectors of three-phase stator or current currents in *qd*0 reference frame
k	PA model order index
$L_{ls,lr}$	per phase winding leakage inductance of stator or rotor
L_m	magnetizing inductance
$L_{sm,rm}$	mutual inductance of stator or rotor
$L_{sr,rs}$	peak value of the stator-to-rotor or rotor-to-stator mutual inductance
$\mathbf{L}_{sr,rs}^{abc}$	matrices of stator-to-rotor or rotor-to-stator mutual inductance in *abc* reference frame
$\mathbf{L}_{sr,rs}^{*abc}$	matrices of modified stator-to-rotor or rotor-to-stator mutual inductance in *abc* reference frame
$L_{ss,rr}$	self-inductance of stator or rotor
$\mathbf{L}_{ss,rr}^{abc}$	matrices of stator or rotor self-inductance in *abc* reference frame
$\mathbf{L}_{ss}^{*abc}$	matrices of modified stator self-inductance in *abc* reference frame

DOI: 10.1002/etep

n	signal data sample index
n_{bb}	number of broken rotor bars
N	number of data samples
N_b	number of total rotor bars
N_s	equivalent stator winding turns
p	number of poles
q	PA model order
r_b	rotor bar resistance
$\Delta r_{ra,b,c}$	resistance change in rotor phase *a, b* or *c*
$\Delta \mathbf{r}_r^{*qd0}$	matrix of rotor resistance changes in *qd0* reference frame
$r_{s,r}$	equivalent one-phase resistance of stator or rotor
$\mathbf{r}_{s,r}$	matrices of three-phase resistances of stator or rotor in *abc* reference frame
$\mathbf{r}_{s,r}^{*}$	matrices of modified three-phase resistances of stator or rotor in *abc* reference frame
$\mathbf{r}_s^{*qd0}$	matrices of modified stator resistances in *qd0* reference frame
$\mathbf{r}_{s,r}^{qd0}$	matrices of three-phase resistances of stator or rotor in *qd0* reference frame
t	time
T_{em}	electromagnetic torque
T_{damp}	damping torque
T_{load}	mechanical load torque
$\mathbf{T}_{qd0}(\theta)$	transformation function
T_s	sample interval
$\mathbf{u}_{s,r}^{abc}$	column vectors of three-phase stator or rotor voltages in *abc* reference frame
$\mathbf{u}_{s,r}^{qd0}$	column vectors of three-phase stator or rotor voltages in *qd*0 reference frame
x	reactance
y	signal
$\mathbf{Y}$	matrix of of data points from $y(1)$ to $y(N-1)$
α_k	damping factors
$\varepsilon(n)$	exponential prediction approximation error of data $y(n)$
ε	column vectors or exponential prediction errors
θ	transformation angle
θ_k	initial phases
θ_r	rotor angle
$\lambda_{s,r}^{abc}$	column vectors of three-phase stator or rotor flux linkages in *abc* reference frame
$\lambda_{s,r}^{qd0}$	column vectors of three-phase stator or rotor flux linkages in *qd*0 reference frame
$\lambda_{s,r}^{*qd0}$	column vectors of modified stator or rotor flux linkages in *qd0* reference frame
ψ	flux linkage per second
ψ_r^{*qd0}	modified column vectors of rotor flux linkage per second in *qd*0 reference frame
ψ_s^{*qd0}	modified column vectors of stator flux linkage per second in *qd*0 reference frame
ω	transformation angular frequency
ω_b	base value of the angular frequency
ω_r	rotor angular frequency

REFERENCES

1. Thomson WT, Rankin D. Case histories of rotor winding fault diagnosis in induction motors. *Proceedings of the 2nd International Conference on Condition Monitoring,* University of Swansea 1987; 798–819.
2. Manolas SJ. Analysis of squirrel cage induction motors with broken bars and rings. *IEEE Transactions on Energy Conversion 1999*; **14**:1300–1305. DOI: 10.1109/60.815063
3. Joksimovic GM, Penman J. The detection of inter turn short circuits in the stator windings of operating motors. *IEEE Transactions on Industrial Electronics 2000*; **47**:1078–1084.
4. Chen S, Zivanovic R. A novel high-resolution technique for induction machine broken bar detection. *AUPEC'07*, Perth, Australia, 9–12 December 2007; 1–5. DOI: 10.1109/AUPEC.2007.4548040

5. Bangura JF, Demerdash NA. Diagnosis and characterization of effects of broken bars and connectors in squirrel-cage induction motors by a time-stepping coupled finite element-state space modeling approach. *IEEE Transactions on Energy Conversion 1999*; **14**:1167–1176. DOI: 10.1109/60.815043
6. Jiang J, Cai Z. Study of the large induction motor modeling to simulate squirrel cage broken bars and rings based on atp. *Proceedings 6th International Conference Advances in Power System Control, Operation and Management, APSCOM 2003*; Hong Kong, 2003; 210–214.
7. Toliyat HA, Lipo TA. Transient analysis of cage induction machines under stator, rotor bar and end ring faults. *IEEE Transactions on Energy Conversion 1995*; **10**:241–247. DOI: 10.1109/60.391888
8. Munoz AR, Lipo TA. Complex vector model of the squirrel-cage induction machine including instantaneous rotor bar currents. *IEEE Transactions on Industry Applications 1999*; **35**:1332–1340. DOI: 10.1109/28.806047
9. Liang B, Ball AD, Iwnicki SD. Simulation and fault detection of three-phase induction motors. *Proceedings TENCON'02 IEEE 2002*; **3**:1813–1817. DOI: 10.1109/TENCON.2002.1182688
10. Benbouzid MEH. A review of induction motors signature analysis as a medium for faults detection. *IEEE Transactions on Industrial Electronics 2000*; **47**:984–993. DOI: 10.1109/41.873206
11. Marple SL. A tutorial overview of modern spectral estimation. *International Conference on Acoustics, Speech and Signal Processing (ICASSP)* 1989; 4: 2152–2157. DOI: 10.1109/ICASSP. 1989.266889
12. Thomson WT, Fenger M. Current signature analysis to detect induction motor faults. *Industry Application Magazine, IEEE 2001*; **7**:26–34. DOI: 10.1109/2943.930988
13. Hargis C, Gaydon BG, Kamash K. The detection of rotor defects in induction motors. *Proceedings of IEEE Conference on Electrical Machines Design and Application* 1982; 216–220.
14. Sen PC. *Principles of Electric Machines and Power Electronics*. John Wiley and Sons: New York, 1989.
15. Krause PC, Wasynczuk O, Sudhof SD. *Analysis of Electric Machinery*. IEEE Press: New York, 1995.
16. Bellini A, Filippetti F, Franceschini G, Tassoni C, Kliman GB. Quantitative evaluation of induction motor broken bars by means of electrical signature analysis. *IEEE Transactions on Industry Application 2001*; **37**:1248–1255. DOI: 10.1109/28.952499
17. Filippetti F, Martelli M, Franceschini G, Tassoni C. Development of expert system knowledge base to on-line diagnosis of rotor electrical faults of induction motors. *Recordings of Conference. IEEE IAS Annual Meeting* Houston, TX, 1992; 92–99. DOI: 10.1109/IAS. 1992.244459
18. Chang X, Cocquempot V, Christophe C. A model of asynchronous machines for stator fault detection and isolation. *IEEE Transactions on Industrial Electronics 2003*; **50**:578–584. DOI: 10.1109/TIE.2003.812471
19. Ong CM. *Dynamic Simulation of Electric Machinery Using MATLAB/SIMULINK*. Prentice Hall: New Jersey, 1998.
20. Santos PM, Correa MBR, Jacobina CB, *et al*. A simplified induction machine model to study rotor broken bar effects and for detection. *PESC'06, 37th IEEE*, 18–22 June 2006; 1–7. DOI: 10.1109/PESC.2006.1712154
21. Cruz SMA, Cardoso AJM. Multiple reference frame theory: a new method for the diagnosis of stator faults in three-phase induction motors. *IEEE Transactions on Energy Conversion 2005*; **20**:611–619. DOI: 10.1109/TEC.2005.847975
22. Ertugrul N. LabVIEW for electric circuits, machines, drives, and laboratories. *National Instruments Virtual Instrumentation Series*. Prentice Hall: Upper Saddle River, NJ, 2002.
23. Prony BGRde. Essai éxperimental et analytique: sur les lois de la dilatabilité de fluides élastique et sur celles de la force expansive de la vapeur de l'alkool, à différentes températures. *Journal de l'École Polytechnique 1795*; **22**:24–76. (in French).
24. Marple SL. *Digital Spectral Analysis with Applications*. Prentice-Hall: New Jersey, 1987.
25. Zivanovic R, Schegner P, Seifert O, Pilz G. Identification of the resonant-grounded system parameters by evaluating fault measurement records. *IEEE Transactions on Power Delivery, 2004*; **19**:1085–1090. DOI: 10.1109/TPWRD.2004.829945
26. Zivanovic R, Chen S, Fault Diagnostics of Induction Machines using Prony Analysis. *IEEE Power Tech Conference* 1–5 July 2007, Lausanne, Switzerland, No. 496.
27. Chen S. Induction machine broken rotor bar diagnostics using Prony Analysis, *Masters Thesis*, School of Electrical & Electronic Engineering, University of Adelaide, Australia, 2008.
28. Arkan M, Kostic-Perovic D, Unsworth PJ. Modelling and simulation of induction motors with inter-turn faults for diagnostics. *Electric Power System Research 2005*; **75**:57–66. DOI: 10.1016/j.epsr.2004.08.015
29. Houdouin G, Barakat G, Dakyo B, Destobbeleer E. A winding function theory based global method for the simulation of faulty induction machines. *IEEE International Conference on Electric Machines and Drives, IEMDC'03 2003*; **1**:297–303.
30. Filippetti F, Franceschini G, Tassoni C, Vas P. AI techniques in induction machines diagnosis including the speed ripple effect. *IEEE Transactions on Industry Application 1998*; **34**:98–108. DOI: 10.1109/28.658729